Nanoscale Res Lett (2009) 4:262–268
DOI 10.1007/s11671-008-9235-0

NANO EXPRESS

Atomic Force Microscopy Study of the Kinetic Roughening in Nanostructured Gold Films on SiO_2

F. Ruffino · M. G. Grimaldi · F. Giannazzo · F. Roccaforte · V. Raineri

Received: 17 November 2008 / Accepted: 18 December 2008 / Published online: 6 January 2009

Abstract Dynamic scaling behavior has been observed during the room-temperature growth of sputtered Au films on SiO_2 using the atomic force microscopy technique. By the analyses of the dependence of the roughness, σ, of the surface roughness power, $P(f)$, and of the correlation length, ξ, on the film thickness, h, the roughness exponent, $\alpha = 0.9 \pm 0.1$, the growth exponent, $\beta = 0.3 \pm 0.1$, and the dynamic scaling exponent, $z = 3.0 \pm 0.1$ were independently obtained. These values suggest that the sputtering deposition of Au on SiO_2 at room temperature belongs to a conservative growth process in which the Au grain boundary diffusion plays a dominant role.

Keywords Dynamic scaling behavior · Kinetic roughening · Atomic force microscopy · Gold · SiO_2

Introduction

Thin films having 0.1 nm thickness play important roles in various fields of modern day science and technology [1, 2]. In particular, the structure and properties of metal films on non-metal surfaces are of considerable interest [3–6] due to their potential applications in various electronic, magnetic, and optical devices. Most of these properties change drastically, when ultrathin films are formed from bulk materials, because of the confinement effects. The study of the morphology of thin films with the variation of thickness gives an idea about the growth mechanism of these films [7, 8]. This indicates the importance of such studies both from basic theoretical understanding and applications points of view. The study of morphology and the understanding of growth mechanisms are also essential to prepare materials in controlled way for the desired properties. Scanning probe microscopy techniques, such as atomic force microscopy (AFM), are important methodologies to study the surface morphology in real space [9–12]. The top surface can be imaged using an AFM and these images provide information about the morphology and the variation of roughness as a function of thickness and scan length. This variation of roughness essentially gives the height–height correlation and can be used to extract the growth mechanism of the film [13].

All rough surfaces exhibit perpendicular fluctuations which are characterized by a rms width $\sigma = <(x,y)^2>^{1/2}$ being $z(x,y) = h(x,y) - <h(x,y)>$ with $h(x, y)$ the height function and $<\ldots.>$ the spatial average over a planar reference surface. Films grown under nonequilibrium condition are expected to develop self-affine surfaces [7, 14], whose rms widths scale with time t and the length L sampled as [15]

$$\sigma(L,t) = L^{\alpha} F\left(t/L^{\alpha/\beta}\right) \quad (1)$$

where $\sigma(L) \propto L^{\alpha}$ for $t/L^{\alpha/\beta} \to \infty$ and $\sigma(t) \propto t^{\beta}$ for $t/L^{\alpha/\beta} \to 0$. The parameter $0 < \alpha < 1$ is defined as the roughness exponent [16], and the parameter, β, as the growth exponent. Actual self-affine surfaces are characterized by an upper horizontal cutoff to scaling, or correlation length, ξ, beyond which the surface width no longer scales as L^{α}, and eventually reaches a saturation

F. Ruffino (✉) · M. G. Grimaldi
Dipartimento di Fisica e Astronomia, MATIS CNR-INFM, Università di Catania, via S. Sofia 64, I-95123 Catania, Italy
e-mail: francesco.ruffino@ct.infn.it

F. Giannazzo · F. Roccaforte · V. Raineri
Consiglio Nazionale delle Ricerche–Istituto per la Microelettronica e Microsistemi, VIII Strada 5, I-95121 Catania, Italy

value, σ. Implicit in Eq. 1 is a correlation length which increases with time as $\xi \propto t^{1/z}$, where $z = \alpha/\beta$ is the dynamic scaling exponent.

In thin films deposition methodologies in which the film thickness, h, is proportional to the time of deposition, t, then, in the asymptotical limits,

$$\sigma(h) = ah^{\beta} \tag{2}$$

$$\xi(h) = bh^{1/z} \tag{3}$$

where a and b are the opportune proportionality constants.

Theoretical treatments of nonequilibrium film growth typically employ partial differential equations involving phenomenological expansions in the derivatives of a time-dependent height function, $h(x, y, t)$. The Kardar–Parisi–Zhang (KPZ) equation [17] and the Siegert–Plischke (SP) equation [8] are examples of this approach. The KPZ equation concerns the nonconservative systems (it does not conserve the particle number): in the nonconservative dynamics the side growth is allowed with the creation of voids and overhangs, but the relaxation mechanisms such as desorption or diffusion are not dominant enough to eliminate these defects completely. The KPZ equation for nonequilibrium and nonconservative systems yields $\alpha = 0.3$–0.4 and $\beta = 0.24$–0.25 for growth of a two-dimensional surface [18, 19]. The SP equation concerns, instead, nonequilibrium but conservative systems. For conservative growth [8, 20–23] the primary relaxation mechanism is the surface diffusion. Because the desorption of atoms and formation of overhangs and voids are negligibly small, the mass and volume conservation laws play an important role in the growth. The SP equation for nonequilibrium and conservative systems yields $\alpha = 1$ and $\beta = 0.25$ for growth of a two-dimensional surface [8]. The values of α and β predicted by the theories for nonconservatives and conservatives systems may vary depending on the couplings with other effects.

Although extensive theoretical studies have predicted many important features in the growth dynamics of thin films, experimental works have to be performed to verify these predictions. In this article, we report an AFM study of the thickness dependence of σ and ξ for a nanostructured thin Au film deposited by sputtering at room temperature on a SiO_2 substrate. By such, studies the value of $\alpha = 0.9 \pm 0.1$ and $\beta = 0.3 \pm 0.1$ are determined. Independently, the value of $1/z = 0.3 \pm 0.1$ is obtained. From these measured values, we suggest that the growth of Au film on SiO_2 at room temperature is consistent with a conservative growth process. A comparison with theoretical and experimental literature data on the growth of thin metal films is finally performed. The Au/SiO_2 system has been chosen for two primary reasons: (1) the Au/SiO_2 interface grows, at room temperature, in the Volmer–Weber mode, and it is unreactive and abrupt [24]. This fact simplifies the experimental analyses allowing to neglect spurious effects on the interface growth deriving from the reaction between the deposited film and the substrate. From this fact, after all, follows that the growth of Au film on SiO_2 at room temperature belongs to the conservative class of dynamic process; (2) The Au/SiO_2 nanostructured system represents a widely investigated material for nanoelectronic applications [25]—in such a system, the reaching of an atomic level control of the structural properties allow a manipulation of the nanoscale electrical ones [25].

Experimental

A cz-<100> silicon wafer (with resistivity, $\rho \approx 6 \times 10^{-3}\,\Omega\,\text{cm}$) was used as starting substrate. It was initially etched in 10% aqueous HF solution to remove the native oxide. Then it was annealed at 1223 K for 15 min in O_2 in order to grow an uniform, 10-nm thick, amorphous SiO_2 layer. A series of Au films were deposited onto the SiO_2 substrate by RF sputtering using an Emitech K550× Sputter coater apparatus. The depositions were performed at room temperature, with a base pressure of 10^{-4} Pa. Samples of increasing nominal Au thickness, h, were deposited: 2 nm (sample 1), 8 nm (sample 2), 14 nm (sample 3), 20 nm (sample 4), 26 nm (sample 5), 32 nm (sample 6). In our experimental deposition conditions, the thickness, h, of the deposited Au film is proportional to the deposition time t: $h = at$ being $a \approx 6.67 \times 10^{-2}$ nm/s. The nominal thickness of the deposited Au film was checked by Rutherford backscattering analyses (using 2 MeV $^4He^+$ backscattered ions at 165°). The evolution of Au film morphology with the thickness, h, was analyzed by AFM using a PSIA XE150 microscope operating in non-contact mode and ultra-sharpened Si tips were used and substituted as soon as a resolution loss was observed during the acquisition. AFM images were analyzed by using the XEI software. The XEI is the PSIA-AFM image processing and analysis program. The XEI software allows users to extract several information from the sample surface by utilizing various analysis tools and also by providing the ability to remove certain artifacts from scan data. For example, its analysis functions include to profile tracer and region, line measurement of height, line profile, power spectrum, line histogram, regional measurement of height, average roughness, volume, surface area, histogram, bearing ratio, and grain analysis functions.

Results and Discussion

The change in morphology of the Au film as a function of its thickness, h, has been followed by AFM. From such analyses, the Au film, in all the samples, results to be formed by spherical nanometric grains of increasing mean size [26]. As an example, Fig. 1 shows 5 × 5 μm AFM representative images of the samples: (a) the starting SiO_2 substrate, (b) sample 1 ($h = 2$ nm), (c) sample 2 ($h = 8$ nm), (d) sample 3 ($h = 14$ nm), (e) sample 4 ($h = 20$ nm), (f) sample 5 ($h = 26$ nm), (g) sample 6 ($h = 32$ nm), respectively. First, we obtained the roughness σ for each sample by the corresponding AFM images using the XEI software. In particular, the value of σ for each sample was calculated by averaging the values obtained by five 5 × 5 μm AFM images (for which the roughness results saturated with the scan size L). The error in σ was deducted by the averaging procedure. Thus, Fig. 2 reports the values of σ obtained as a function of h: the experimental data (dots) were fitted by Eq. 2 (continuous line) obtaining the growth exponent $\beta = 0.3 \pm 0.1$.

Furthermore, for each sample we calculated also the averaged power spectrum from the spectra of each of the 512 linear traces. Thus, in contrast to σ, the power spectra are calculated from one-dimensional cross sections of the surface. Each spectrum is the square of the surface roughness amplitude per spatial frequency interval and the integral over all frequencies is the mean-square surface roughness within the measured bandwidth (σ^2). Thus, Fig. 3 reports the calculated surface roughness power, P, as a function of the frequency, f, concerning the representative AFM images presented in Fig. 1: Figure 3a for the sample 1 ($h = 2$ nm), Fig. 3b for the sample 2 ($h = 8$ nm), Fig. 3c for the sample 3 ($h = 14$ nm), Fig. 3d for the sample 4 ($h = 20$ nm), Fig. 3e for the sample 5 ($h = 26$ nm), and Fig. 3f for the sample 6 ($h = 32$ nm), respectively.

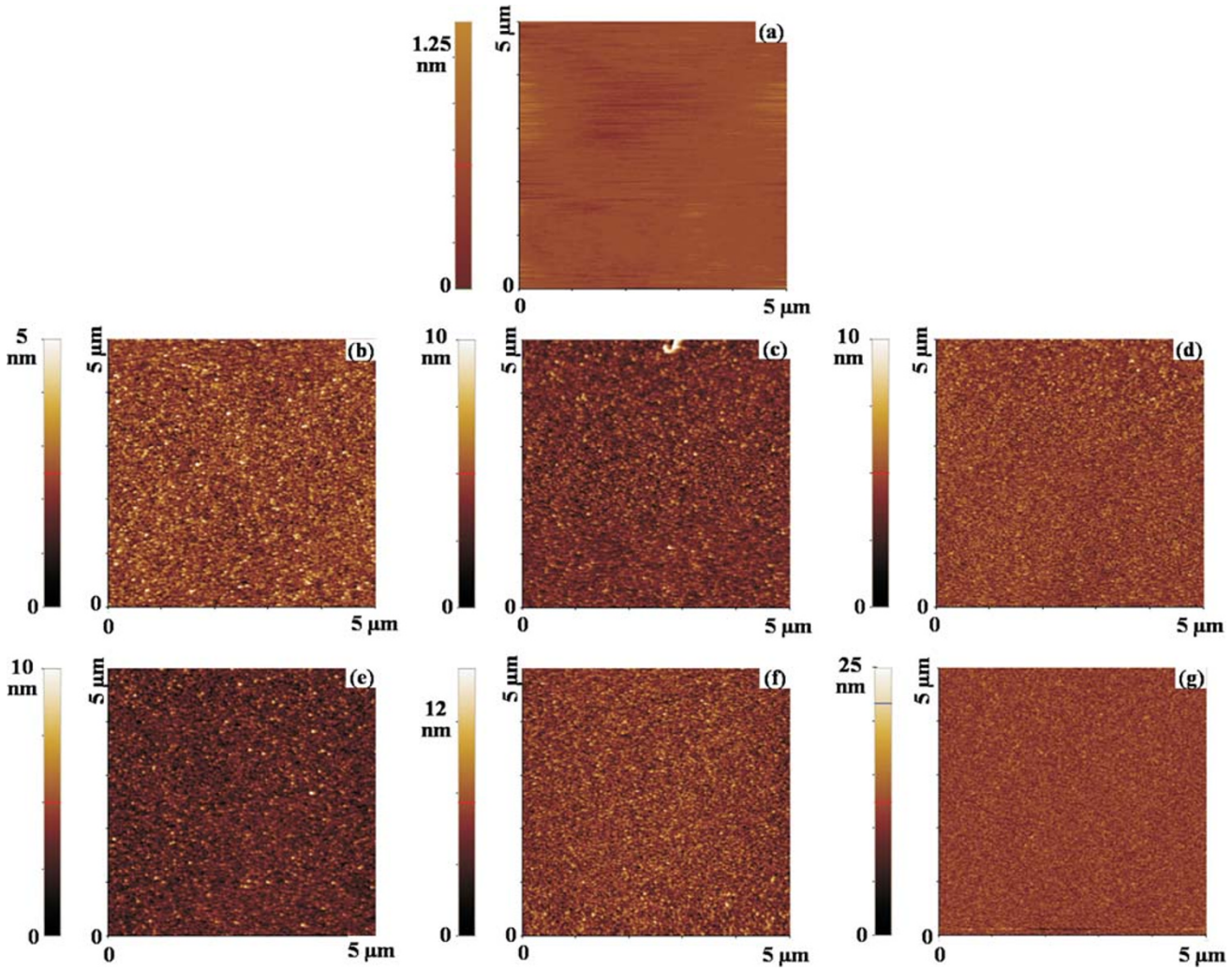

Fig. 1 **a** AFM image (5 μm × 5 μm scan size) of the starting thermal SiO_2 substrate. **b–g** AFM images (5 μm × 5 μm scan size) of the Au film deposited on thermal SiO_2 with different thickness: **b** 2 nm, **c** 8 nm, **d** 14 nm, **e** 20 nm, **f** 26 nm, **g** 32 nm

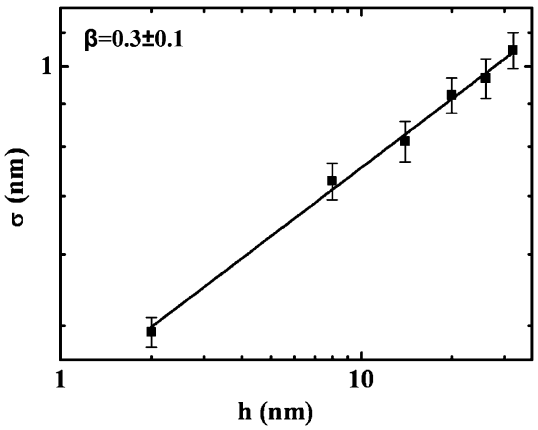

Fig. 2 Experimental (dots) values of the saturated surface roughness of the Au film as a function of the film thickness and fit (continuous line) by Eq. 2. The fit parameter β resulted $\beta = 0.3 \pm 0.1$

The power spectra in Fig. 3 have two distinct regions. The flat, low frequency part resembles uncorrelated white noise. The sloped portion represents the correlated portion of the surface roughness. To obtain the roughness exponent α from this data, we fit the power law decay (in the linear region in the log–log plot) to

$$P\left(f > \xi^{-1}\right) = \frac{const}{f^{\gamma}} \tag{4}$$

and for $\gamma \geq d'$ [27]

$$\alpha = \frac{\gamma - d'}{2} \tag{5}$$

where d' is the dimension of the cross section through the data, which in this case equals 1. Figure 3 reports for each power spectra the fit by Eq. 4 of the linear region (continuous lines). The values of γ_i were obtained by averaging the values obtained by five power spectra corresponding to five 5×5 μm AFM images for each sample. So we obtain the values $\gamma_1 = \gamma(h = 2\text{ nm}) = 2.4 \pm 0.1$, $\gamma_2 = \gamma(h = 8\text{ nm}) = 2.6 \pm 0.1, \gamma_3 = \gamma(h = 14\text{ nm}) = 3.4 \pm 0.2, \gamma_4 = \gamma(h = 20\text{ nm}) = 3.3 \pm 0.1$, $\gamma_5 = \gamma(h = 26\text{ nm}) = 2.2 \pm 0.1$, and $\gamma_6 = \gamma(h = 32\text{ nm}) = 2.9 \pm 0.1$ for the samples 1,

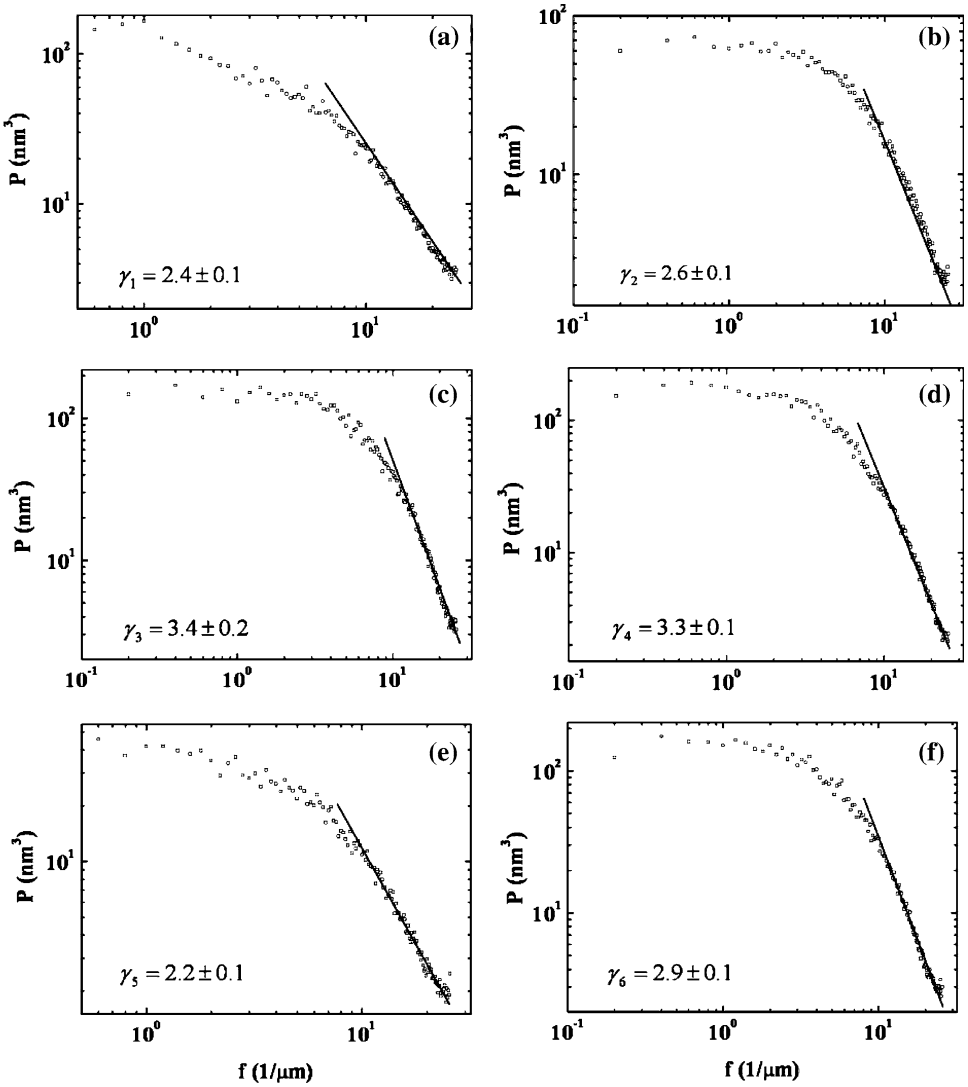

Fig. 3 Representative surface roughness power spectra for the analyzed sample calculated by the AFM images reported in Fig. 1: **a** for the sample with a thickness of 2 nm **b** of 8 nm, **c** of 14 nm, **d** of 20 nm, **e** of 26 nm, **f** of 32 nm of Au respectively. The continuous lines represent the fit by Eq. 4. The values of γ_i reported as insets are calculated by such fits

2, 3, 4, 5, and 6, respectively. Using Eq. 5 the corresponding values of α_i were obtained. The value of the roughness exponent α was obtained as the mean value: $\alpha = 0.9 \pm 0.1$.

By the values of $\beta = 0.3 \pm 0.1$ and $\alpha = 0.9 \pm 0.1$ previously derived, the value of the dynamic scaling exponent $z = \alpha/\beta = 2.9 \pm 0.4$ (or alternatively of $1/z = 0.3 \pm 0.1$) is predicted. But now -z can be derived by the experimental data to try confirmation of the theoretical predicted value. In fact, to characterize the scale of correlations perpendicular to the growing direction, the correlation frequency ξ^{-1} can be used. It can be evaluated by the power spectra as the spatial frequency where $P(f)$ has fallen to $1/e$ of its saturation low frequency value and above which σ is correlated. Using the five power spectra for each sample already used for the calculation of the γ_i and performing the averaging procedure, the values of $\xi_1 = \xi(h = 2\text{ nm}) = (0.076 \pm 0.010)\mu\text{m}$, $\xi_2 = \xi(h = 8\text{ nm}) = (0.122 \pm 0.098)\mu\text{m}$, $\xi_3 = \xi(h = 14\text{ nm}) = (0.139 \pm 0.095)\mu\text{m}$, $\xi_4 = \xi(h = 20\text{ nm}) = (0.159 \pm 0.010)\mu\text{m}$, $\xi_5 = \xi(h = 26\text{ nm}) = (0.178 \pm 0.009)\mu\text{m}$, $\xi_6 = \xi(h = 32\text{ nm}) = (0.189 \pm 0.096)\mu\text{m}$ for the correlation lengths for the samples 1, 2, 3, 4, 5, and 6, respectively, were obtained. Figure 4 reports as dots, in a log–log scale, such values as a function of the film thickness, h. The continuous line is the fit by Eq. 3 allowing the determination of $1/z = 0.3 \pm 0.1$ in agreement with the predicted value. Finally, from the AFM analyses reported in Fig. 1, statistical data on the radius, area and volume of the Au nanometric grains forming the film can be obtained. The XEI software for the analyses of the AFM images allow to obtain the distribution of the grains radii, R, and of the grains areas S by a procedure consisting in the definition of each grain area by the surface image sectioning of a plane that was positioned at the half grain height. As a consequence, the distribution of the grains radii R, surface areas, S, and volumes, V can be extracted. By such distributions, the mean grain radius, $\langle R \rangle$, the mean grain area, $\langle S \rangle$, and the mean grain volume $\langle V \rangle$ can be extracted with the respective statistical errors.

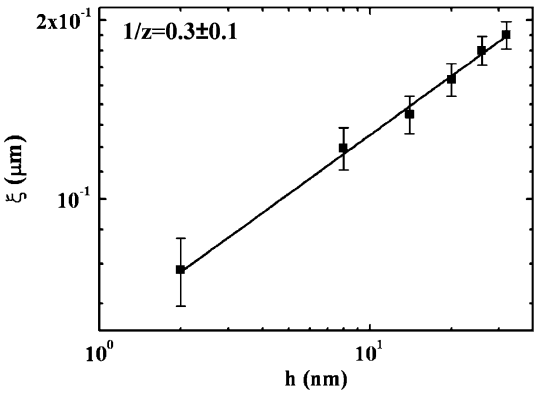

Fig. 4 Experimental (dots) values of the correlation length for the Au film as a function of the film thickness and fit (continuous line) by Eq. 3. The fit parameter $1/z$ resulted $1/z = 0.3 \pm 0.1$

Therefore, Fig. 5a–c report $\langle R \rangle$, $\langle S \rangle$, and $\langle V \rangle$ as a function of the film thickness h. As a final remark, it is worth to note that Fig. 5c, being $\langle V \rangle \propto \langle R \rangle^3$ indicates clearly a grain growth scaling law $\langle R \rangle \propto h^{1/3}$. Since the dynamical scaling theories predict $\langle R \rangle \propto h^{1/z}$ [8] then also such a data conduct to the results $z = 3$ for the dynamic scaling exponent.

Now, we turn to the comparison of the data presented in this study with experimental and theoretical literature studies. The values obtained by us in this study are comparable to those reported by Chevrier et al. [28] ($\beta = 0.25$–0.32) for vapor-deposited Fe on Si at 323 K, by G. Palasantzas and J. Krim [29] ($\alpha = 0.82 \pm 0.05$, $\beta = 0.29 \pm 0.06$ and $z = 2.5 \pm 0.5$) for room-temperature vapor-deposited Ag film on quartz. But they do not coincide with the values reported by You et al. [30] ($\alpha = 0.42$, $\beta = 0.40$) for room-temperature sputtered Au film on Si, to those reported by Fanfoni et al. [31] and Placidi et al. [32] for the molecular beam epitaxy

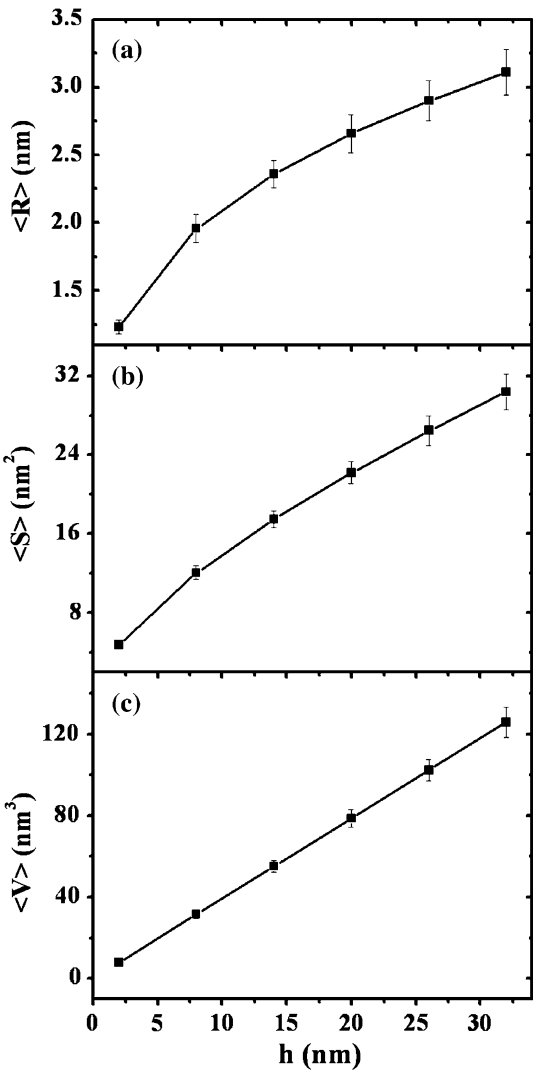

Fig. 5 Experimental evolution (dots) of the mean grain radius $\langle R \rangle$ (**a**), mean grain surface area $\langle S \rangle$ (**b**), and mean grain volume $\langle V \rangle$ (**c**) as a function of the thickness film h. The lines are only guide for the eyes

dynamical growth of silver islands on GaAs(001)-(2 × 4) ($z = 1.5 \pm 0.2$ and $z = 4.2 \pm 0.4$, respectively) and to those reported by Rosei et al. [33] for reactive-deposited Ge on Si(1111) ($z = 0.70 \pm 0.20$). We can attribute the difference of our results from those of You et al. to the different used substrates used since though Au is unreactive with SiO_2, it is reactive with Si [34] and to the lower substrate temperature. The difference with respect to the values of Fanfoni et al., Placidi et al. and Rosei et al. can be attributed to differences in film deposition conditions. We believe that our values of $\alpha = 0.9 \pm 0.1$, $\beta = 0.3 \pm 0.1$ and $1/z = 0.3 \pm 0.1$ for room-temperature sputtered Au films are more consistent with a conservative deposition process (i.e. prediction of the SP equation) rather than a nonconservative one (i.e. prediction of the KPZ equation). Other experiments that characterize self-affine fractals using different techniques [35–37] indicate that the values of α measured from metal thin films range from 0.65 to 0.95, which are indeed higher than that predicted by the nonconservative growth models [17–19]. The exponents obtained in this experiment are thus more consistent with the results of conservative growth models [20–23]. A justification of this fact can be found in the microscopic mechanism governing the Au film growth on SiO_2 at room temperature. Our recent data [26] suggest that during the Au sputter deposition at room temperature the film growth is driven by the Au grain boundary diffusion with a diffusion coefficient $D_{gb}(300\ \mathrm{K}) \approx 2 \times 10^{-17}\ \mathrm{cm}^2/\mathrm{s}$ (rather than an Au surface diffusion, since the surface diffusion coefficient of Au on SiO_2 is very small at room temperature, $D_{\mathrm{Au/SiO_2}}(300\ \mathrm{K}) \approx 7 \times 10^{-26}\ \mathrm{cm}^2/\mathrm{s}$ [24]). In fact, the AFM analyses in connection with transmission electron microscopy analyses allow to conclude that the Au film is formed by three-dimensional nanometric grains that grows as "normal grains" for thickness in the 0.33 nm. For higher thickness, together with the normal grain growth, the growth of "abnormal large grains" is observed. The normal grain growth appears to be (at room temperature) controlled by Au diffusion on grain boundaries (rather than by Au surface diffusion) while the abnormal grain growth process appears to be driven by the differences between surface energies of the normal and abnormal grains, so that grains with favored orientations grow at a higher rate (with respect to the normal grain growth rate) by annihilating the surrounding normal grains. We believe, thus, that, during the deposition process, the overhangs and voids are unlikely to appear in the growth of the film because the Au grain boundary diffusion plays a dominant role.

Conclusion

An AFM study of the dynamic evolution of a growing interface was carried out for room-temperature Au sputtered onto a SiO_2 substrate. The analyses of AFM images of the Au film allowed us to derive the roughness, σ, the surface roughness power, $P(f)$, and the correlation length, ξ, as a function of the film thickness, h. Analyzing such dependences the roughness exponent, the growth exponent and the dynamic scaling exponent were independently obtained: $\alpha = 0.9 \pm 0.1$, $\beta = 0.3 \pm 0.1$ and $z = 3.0 \pm 0.1$. These values suggest that the sputtering deposition of Au on SiO_2 at room temperature belongs to a conservative growth process in which the Au grain boundary diffusion plays a dominant role. This study suggests further analyses concerning, for example, the dependence of the exponents α, β, and z on the substrate temperature during the film deposition (such as pointed out in the experimental study of You et al. [30] for the case of Au on Si), on the rate deposition (such as pointed out by Collins et al. [38]) and the extension of the experimental investigation to other systems that could present nonequilibrium conservative or nonconservative dynamical growth mechanisms (e.g., Pd/SiO_2, Au/SiC, Pd/SiC, Au/GaN, Pd/GaN, Pd/Si).

References

1. M. Ohring, *The Materials Science of Thin Films* (Academic Press, New York, 1992)
2. D.L. Smith, *Thin Film Deposition* (McGraw-Hill, New York, 1995)
3. W.G. Schmidt, F. Bechstedt, G.P. Srivastava, Surf. Sci. Rep. **25**, 141 (1996). doi:10.1016/S0167-5729(96)00006-4
4. C.T. Campbell, Surf. Sci. Rep. **27**, 1 (1997). doi:10.1016/S0167-5729(96)00011-8
5. S. Shanmugam, B. Viswanathan, T.K. Varadarajan, Nanoscale Res. Lett. **2**, 175 (2007). doi:10.1007/s11671-007-9050-z
6. P.S. Kishore, B. Viswanathan, T.K. Varadarajan, Nanoscale Res. Lett. **3**, 14 (2008). doi:10.1007/s11671-007-9107-z
7. A.-L. Barabasi, H.E. Stanley, *Fractal Concepts in Surface Growth* (Cambridge University Press, Cambridge, 1995)
8. M. Siegert, M. Plischke, Phys. Rev. Lett. **73**, 1517 (1994). doi:10.1103/PhysRevLett.73.1517
9. R. Wiesendanger, *Scanning Probe Microscopy and Spectroscopy* (Cambridge University Press, Cambridge, 1994)
10. D. Sarid, *Scanning Force Microscopy with Applications to Electric, Magnetic and Atomic Forces* (Oxford University Press, Oxford, 1994)
11. S.-R. Jian, I.-Ju. Teng, P.-F. Yang, Y.-S. Lai, J.-M. Lu, J.-G. Chang, S.-P. Ju, Nanoscale Res. Lett. **3**, 186 (2008). doi:10.1007/s11671-008-9134-4
12. S.-R.- Jian, J.-Y. Juang, Nanoscale Res. Lett. **3**, 249 (2008). doi:10.1007/s11671-008-9144-2
13. J.K. Basu, S. Hazra, M.K. Sanyal, Phys. Rev. Lett. **82**, 4675 (1999). doi:10.1103/PhysRevLett.82.4675
14. F. Family, T. Vicsek, *Dynamics of Fractals Surfaces* (World Scientific, Singapore, 1991)
15. F. Family, T. Vicsek, J. Phys. A **18**, L75 (1985). doi:10.1088/0305-4470/18/2/005
16. J. Krim, J.O. Indekeu, Phys. Rev. E Stat. Phys. Plasmas Fluids Relat. Interdiscip. Topics **48**, 1576 (1993). doi:10.1103/PhysRevE.48.1576

17. M. Kardar, G. Parisi, Y.-C. Zhang, Phys. Rev. Lett. **56**, 889 (1986). doi:10.1103/PhysRevLett.56.889
18. J.M. Kim, J.M. Kosterlitz, Phys. Rev. Lett. **62**, 2289 (1989). doi:10.1103/PhysRevLett.62.2289
19. B.M. Forrest, L.-H. Tang, Phys. Rev. Lett. **64**, 1405 (1990). doi:10.1103/PhysRevLett.64.1405
20. J. Villain, J. Phys. I **1**, 19 (1991)
21. D.E. Wolf, J. Villain, Europhys. Lett. **13**, 389 (1990). doi:10.1209/0295-5075/13/5/002
22. Z.-W. Lai, S. Das Sarma, Phys. Rev. Lett. **66**, 2348 (1991). doi:10.1103/PhysRevLett.66.2348
23. L.-H. Tang, T. Nattermann, Phys. Rev. Lett. **66**, 2899 (1991). doi:10.1103/PhysRevLett.66.2899
24. F. Ruffino, A. Canino, M.G. Grimaldi, F. Giannazzo, C. Bongiorno, F. Roccaforte, V. Raineri, J. Appl. Phys. **101**, 064306 (2007). doi:10.1063/1.2711151
25. F. Ruffino, M.G. Grimaldi, F. Giannazzo, F. Roccaforte, V. Raineri, Appl. Phys. Lett. **83**, 263108 (2006). doi:10.1063/1.2424433
26. F. Ruffino, C. Bongiorno, F. Giannazzo, F. Roccaforte, V. Raineri, C. Spinella, V. Raineri, J. Appl. Phys. (submitted)
27. R.F. Voss, in *Scaling Phenomena in Disordered Systems*, ed. by R. Pynn, A. Skejeltorp (Plenum, New York, 1985)
28. J. Chevrier, V. Le Thanh, R. Buys, J. Derrien, Eoruphys. Lett. **16**, 737 (1991). doi:10.1209/0295-5075/16/8/006
29. G. Palasantzas, J. Krim, Phys. Rev. Lett. **73**, 3564 (1994). doi:10.1103/PhysRevLett.73.3564
30. H. You, R.P. Chiarello, H.K. Kim, K.G. Vandervoort, Phys. Rev. Lett. **70**, 2900 (1993). doi:10.1103/PhysRevLett.70.2900
31. M. Fanfoni, E. Placidi, F. Arciprete, F. Patella, N. Motta, A. Balzarotti, Surf. Sci. **445**, L17 (2000). doi:10.1016/S0039-6028(99)01099-7
32. E. Placidi, M. Fanfoni, F. Arciprete, F. Patella, N. Motta, A. Balzarotti, Mater. Sci. Eng. B **69–70**, 243 (2000). doi:10.1016/S0921-5107(99)00303-7
33. F. Rosei, N. Motta, A. Sgarlata, G. Capellini, F. Boscherini, Thin Solid Films **36**, 29 (2000). doi:10.1016/S0040-6090(00)00829-4
34. J.F. Chang, T.F. Young, Y.L. Yang, H.Y. Ueng, T.C. Chang, Mater. Chem. Phys. **83**, 199 (2004). doi:10.1016/S0254-0584(03)00240-2
35. R.P. Chiarello, V. Panella, J. Krim, C. Thompson, Phys. Rev. Lett. **67**, 3408 (1991). doi:10.1103/PhysRevLett.67.3408
36. M.W. Mitchell, A. Bonnell, J. Mater. Res. **5**, 2244 (1990). doi:10.1557/JMR.1990.2244
37. J.M. Gómez-Rodriguez, A.M. Baró, R.C. Salvezza, J. Vac. Sci. Technol. B **9**, 495 (1991). doi:10.1116/1.585554
38. G.W. Collins, S.A. Letts, E.M. Fearon, R.L. McEachern, T.P. Bernat, Phys. Rev. Lett. **73**, 709 (1994)